A Self-Calibrating Radar Sensor System for Measuring Vital Signs

Ming-Chun Huang, *Member, IEEE*, Jason J. Liu, *Member, IEEE*, Wenyao Xu, *Member, IEEE*, Changzhan Gu, *Member, IEEE*, Changzhi Li, *Senior Member, IEEE*, and Majid Sarrafzadeh, *Fellow, IEEE*

***Abstract*—Vital signs (i.e., heartbeat and respiration) are crucial physiological signals that are useful in numerous medical applications. The process of measuring these signals should be simple, reliable, and comfortable for patients. In this paper, a noncontact self-calibrating vital signs monitoring system based on the Doppler radar is presented. The system hardware and software were designed with a four-tiered layer structure. To enable accurate vital signs measurement, baseband signals in the radar sensor were modeled and a framework for signal demodulation was proposed. Specifically, a signal model identification method was formulated into a quadratically constrained ℓ_1 minimization problem and solved using the upper bound and linear matrix inequality (LMI) relaxations. The performance of the proposed system was comprehensively evaluated using three experimental sets, and the results indicated that this system can be used to effectively measure human vital signs.**

***Index Terms*—Calibration, Doppler radar, vital sign measurement.**

I. Introduction

AMONG the various medical signals, vital signs (e.g., heart rate and respiratory rate) are the most crucial measures used to assess bodily functions and monitor illness progression to determine the effective treatments that should be administered [14]. Furthermore, vital signs measurement is helpful in predicting potential clinical events. For example, the variation in respiratory rate is a marker for cardiac arrest or admission to an intensive care unit [13].

Several off-the-shelf home devices are used measuring vital signs [20], [35]. They require users to follow the instrument instructions strictly and to perform the measurement under controlled conditions. For example, when a person uses an electrocardiography (ECG) device to measure heartbeat, the electrode should be attached on the correct parts of the body and the person should not move while conducting the measurement. Therefore, consistently obtaining valid vital signs measurement without the assistance of medical personnel is difficult. Moreover, because using these devices is inconvenient, patients are unlikely to perform vital signs measurement by themselves.

For years, the research community has investigated *unobtrusive* methods for vital signs measurement. Generally, existing work can be classified into three categories. The first category is based on direct skin contact. During measurement, a device must be in direct physical contact with the body of the user. Valchinov *et al.* developed a dry skin electrode that reduced contact impedance and variation and motion artifacts [43]. Huang *et al.* [27] designed a portable ECG acquisition system using multiple dry skin electrodes. The second category is based on indirect contact (i.e., sensors that do not require direct physical skin contact). Under-bed mattress sensors have been used to measure heartbeat, respiration, and body movements using thin, air-sealed [44], film [2], hydraulic [26], e-textile [46] pressure sensors. Liu *et al.* [33] introduced a dense e-textile pressure sensor array to estimate the sleep postures and stages. Steffen *et al.* [40] designed magnetic bio-impedance monitoring and capacitive electrocardiogram (ECG) recording systems for heart and lung activity monitoring. Chi *et al.* [12] developed a capacitive electrode to measure heart rate that can function through clothing. The third category is based on noncontact techniques. Noncontact techniques enable monitoring vital signs remotely and seem appealing for users. Aoki *et al.* [1] discussed a nonrestrictive visual sensing method for detecting respiration patterns by using a fiber grating camera and processor unit. Zhu *et al.* [49] developed an infrared-camera-based system to monitor respiration and infer the associated heart rate. Zito *et al.* [51] designed UWB pulse radar sensor for contactless respiratory rate monitoring. Chekmenev *et al.* [10] used a thermal camera consisting of a focal plane array for a long-wave infrared sensor to extract heart rate and respiration from temperature changes. However, all of the aforementioned noncontact methods involve using sensors that are sensitive to changes in environmental factors such as light or temperature, and no robust calibration methods for compensating for these changes have been developed.

In this paper, a low-cost microwave Doppler radar-based system complementary to existing noncontact techniques is presented. According to Doppler theory [5], signals reflected by objects exhibit a quantitative phase change, called Doppler shift, because of the movement of the objects. The magnitude

Manuscript received August 07, 2014; revised January 23, 2015; accepted March 01, 2015. Date of publication May 19, 2015; date of current version February 29, 2016. This work was supported in part by NSF ECCS-1254838/CNS-1423061. This paper was recommended by Associate Editor S. Leonhardt.

M.-C. Huang is with the Department of Electrical Engineering and Computer Science, Case Western Reserve University, Cleveland, OH 44106 USA.

J. J. Liu and M. Sarrafzadeh are with the Department of Computer Science, University of California, Los Angeles, Los Angeles, CA 90066 USA.

W. Xu is with the Department of Computer Science and Engineering, State University of New York at Buffalo, Buffalo, NY 14260 USA (e-mail: wenyaoxu@buffalo.edu).

C. Gu and C. Li are with the Department of Electrical and Computer Engineering, Lubbock, TX 79409 USA.

Color versions of one or more of the figures in this paper are available online at http://ieeexplore.ieee.org.

Digital Object Identifier 10.1109/TBCAS.2015.2411732

1932-4545 © 2015 IEEE. Personal use is permitted, but republication/redistribution requires IEEE permission.
See http://www.ieee.org/publications_standards/publications/rights/index.html for more information.

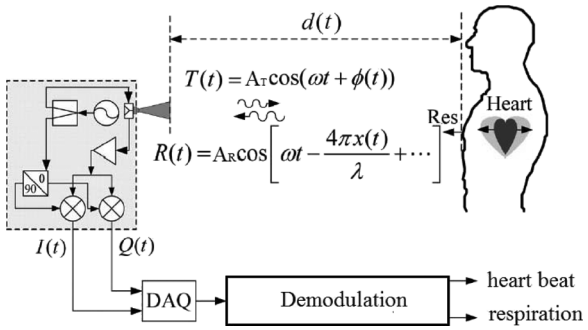

Fig. 1. The I/Q Doppler radar block diagram for non-contact vital signs monitoring.

of the phase change is sufficiently large for measuring heartbeat and chest wall movement. A novel framework based on the Doppler radar structure and signal model was proposed to automatically demodulate the Doppler radar signals and extract the heart and respiratory rates without precalibration. Therefore, this method is a low-cost, reliable solution for noncontact vital signs measurement that is easy to set up.

The remainder of the paper is organized as follows. In Section II, the background of Doppler radar and related studies on radar signal processing are briefly introduced. The layered architecture of the Doppler radar motion-sensing system is described in Section III. In Section IV the challenges and framework of vital signs measurement are addressed. The experimental design, performance evaluation and analyses are discussed in Section V. Finally, the future work is outlined and a conclusion is provided in Section VI.

II. Doppler Radar Preliminaries

The Doppler effect was proposed by Christian Doppler in 1842 and has since been widely applied in motion detection. Microwave Doppler radar was first applied to measure respiratory rate and detect sleep apnea in 1975 [32]. A Doppler radar transmits a continuous-wave signal, which is reflected by a target and then received and demodulated by a receiver. According to Doppler theory, the position-varying information is proportionally demodulated in the reflected signal when the net velocity is zero. Therefore, the chest wall movement caused by volume change during respiration can be detected using the Doppler radar motion-sensing system. Because of the advances in wireless transmission and electronic devices, using in-phase and quadrature (I/Q) Doppler radar for heartbeat detection is feasible [11], [17].

A. In-phase/Quadrature (I/Q) Doppler Radar

Fig. 1 shows the operation theory and block diagram of an I/Q Doppler radar for non-contact vital signs measurement. The Doppler radar system transmits the continuous-wave signal $T(t)$

$$T(t) = A_T \cos\left(\omega t + \phi(t)\right) \tag{1}$$

where A_T is the amplitude of the carrier signal, $\omega = 2\pi f$ denotes the angular velocity (carrier frequency), and $\phi(t)$ represents the time-varying phase information of the transmitted signal.

The subject is at a distance d_0 from the radar and the total traversal distance of microwave signal is $d(t) = 2(d_0 + x(t))$, where $x(t)$ is the time-varying displacement caused by heart beat and respiration.

The transmission wave is reflected by the subject and received at Doppler radar as $R(t)$

$$R(t) = A_R \cos\left[\omega t - \frac{4\pi d_0}{\lambda} - \frac{4\pi x(t)}{\lambda} + \phi\left(t - \frac{2d_0}{c}\right)\right] \tag{2}$$

where A_R is the amplitude of the received signal, $\lambda = c/f$ is the wavelength of the carrier signal, and c is the speed of light [17], [31]. We can see that the time-varying displacement $x(t)$ is modulated in the phase change of the received signal. As shown in Fig. 1, $R(t)$ is down-converted by $T(t)$ and then generates two baseband signals. One is the in-phase signal, denoted by $I(t)$

$$I(t) = A_I \cos\left[\frac{4\pi x(t)}{\lambda} + \frac{4\pi d_0}{\lambda} + \phi\left(t - \frac{2d_0}{c}\right)\right] + DC_I \tag{3}$$

and the other is the quadrature signal, denoted by $Q(t)$

$$Q(t) = A_Q \sin\left[\frac{4\pi x(t)}{\lambda} + \frac{4\pi d_0}{\lambda} + \phi\left(t - \frac{2d_0}{c}\right) + \phi_0\right] + DC_Q \tag{4}$$

where A_I is the amplitude of in-phase signal, A_Q the amplitude of quadrature signal, and ϕ_0 is the phase offset between $I(t)$ and $Q(t)$. DC_I and DC_Q are the DC offsets in I/Q channels, respectively. The ratio between A_I and A_Q is called gain imbalance, and ϕ_0 is called phase imbalance. Both gain imbalance and phase imbalance are caused by multiple factors such as circuit imperfection.

$I(t)$ and $Q(t)$ are then digitized by the data acquisition block (DAQ), and the phase change, $x(t)$, is demodulated for heart beat and respiration measurement. For the simplicity of presentation, we neglect the constant phase offset, $4\pi d_0/\lambda + \phi(t - 2d_0/c)$, in the I/Q receiver and use the following equations to describe the baseband signals.

$$I(t) = A_I \cos\left(\frac{4\pi x(t)}{\lambda}\right) + DC_I \tag{5}$$

and

$$Q(t) = A_Q \sin\left(\frac{4\pi x(t)}{\lambda} + \phi_0\right) + DC_Q \tag{6}$$

B. The Challenge

As shown in Fig. 1, the demodulation module processes the baseband signals, $I(t)$ and $Q(t)$, for heartbeat and respiration information extraction. It is critical to minimize the effect of gain and phase imbalance in practice (i.e., A_I in (5) is equal to A_Q in (6), and ϕ_0 in (6) is equal to zero).

Based on these ideal-case assumptions, several techniques have been proposed in the extant literature for demodulating Doppler radar signals to extract vital signs. Droitcour *et al.* approximated I/Q signals as linear formulas when the responding phase was small, and then extracted vital signs by using the tuning carrier frequency [17]. Tao *et al.* converted transmission waves to a set of pulse signals and detected the phase change according to its peaks [42], whereas Lee *et al.* proposed a reassigned joint time-frequency transform to track the heart rate [29].

Lubecke *et al.* presented various demodulation methods involving the precalibration of DC offsets [6], [34], [36]. Li and Lin formulated I/Q signals into a complex vector to perform Fourier analysis, and the phase change was calculated using iterative spectrum comparison [30].

These existing demodulation methods have two main drawbacks. First, these methods require either approximating I/Q signals [17], [42] or accurately precalibrating the DC offsets [30], [36]. Both the electronic components and multichannel transmission and reflection, which is related to the environment, produce DC offset. Therefore, the DC offsets in the I/Q channels must be recalibrated whenever the environment changes, which is not applicable in practice. Fletcher and Han used dual beams to target various locations; one location was used as a reference [19]. Second, these methods involve the assumption that circuit components are perfect in that the gain and phase imbalances are minimal. In real radar systems, the effect of gain and phase imbalance is considerable. Park *et al.* [37] measured the imbalance factors in a direct-conversion quadrature radar circuit and reported that imbalance is unavoidable. In their experiments, the gain imbalance was 4.7 and the average phase imbalance was 18.5 degrees. Thus, phase imbalance has a severe negative effect on the error rate of signal demodulation [50]. Therefore, developing an accurate and robust signal-processing technique for signal demodulation in Doppler radar systems is necessary. Associated research challenges are listed below.

1) Accuracy: the demodulation method should account for all parameters (i.e., A_I, A_Q, ϕ_0, DC_I, and DC_Q) in the signal model and directly extract the motion component $x(t)$ accurately from the I/Q signals;
2) Self-calibration: external environment might change during sensor measurements. The proposed demodulation method allows signal model recalculation and tolerates possible parameters variance, without manual intervention.

III. System Overview

In this section, the proposed Doppler radar system for non-contact self-calibrating vital signs measurement is introduced. Fig. 2 shows an overview of the structure of this system, which comprises four layers: the sensor, preprocessing, modeling, and information layers. The sensor layer and preprocessing layer were built on the hardware, whereas the modeling layer and information layer were designed using software. Each of the layers are described in the following subsections. A hardware prototype of the radar sensor is shown in Fig. 3 with its main functional components. After preprocessing the sensed baseband radar signal, an elliptic phase model was constructed and

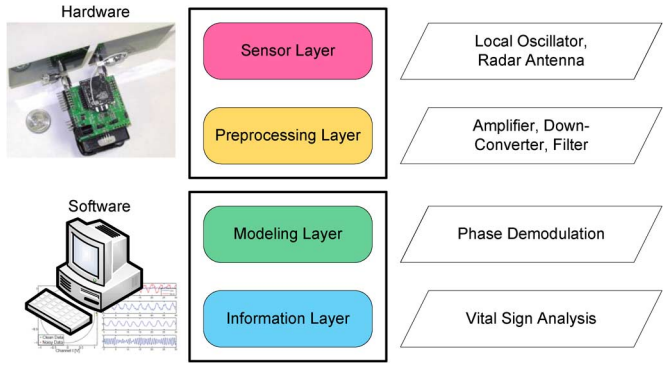

Fig. 2. The layered structure of non-contact self-calibrating vital signs measurement system, including sensor layer, pre-processing layer, modeling layer and information layer.

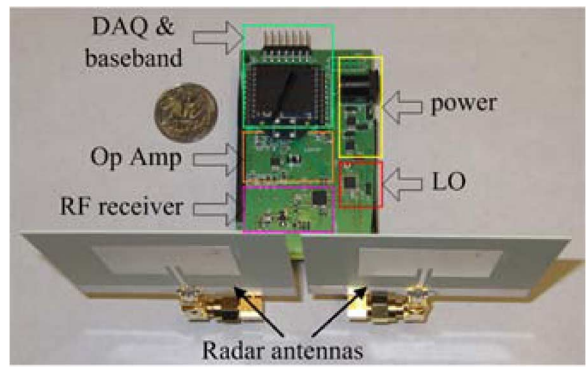

Fig. 3. The hardware prototype of the Doppler radar vital signs measurement system.

the model parameters were calculated based on the proposed min-ℓ_1-based fitting (self-calibration). In the information layer, these self-calibrated elliptic parameters were identified to reconstruct baseband signals, perform demodulation to identify the corresponding chest wall movement, and extract respiration and heartbeat signals using spectrum analysis. The framework of self-calibration (modeling layer) and vital signs extraction (information layer) is shown in Fig. 4.

A. Sensor Layer

The sensor layer generated a single-tone carrier signal that was transmitted to the target to gather the desired phase information [24], [32]. The key building blocks used in the sensor system are shown in Table I. The radar sensor system was designed using a homodyne transceiver architecture integrated on a Rogers 4350 laminate for enhanced radio frequency (RF) performance. In this design, the sensor layer was implemented using a voltage-controlled oscillator (VCO). The single-tone signal produced by the VCO was divided by a balun into two components. One component was transmitted through a transmitter antenna to the target, and the second component served as the local oscillator (LO) signal sent to the demodulator. If the target was moving (e.g., the chest wall of the subject), then the single-tone carrier signal was modulated in the phase containing the movement information of the target, which is a process called nonlinear phase modulation [22], [23]. Although

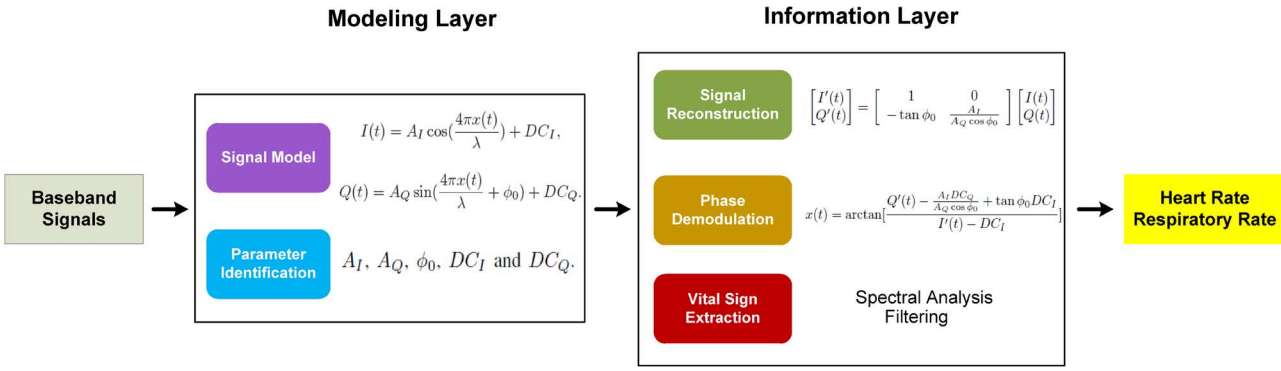

Fig. 4. The framework of signal demodulation in non-contact vital signs monitoring systems.

TABLE I
BUILDING BLOCKS OF THE RADAR-SENSING SYSTEM

Blocks	Manufacturer	Specification
VCO	Hittite	2.25-2.5GHz; Pout: 4.5dBm
Demodulator	Skyworks	RF/LO: 0.4 3GHz; Gain: 1.2dB
LNA	Hittite	2.3-2.5GHz; NF: 1.7dB; Gain: 19dB; P_{1dB}out: 6dBm
Gain Block	RFMD	Gain: 12dB; P_{1dB}out: 11dBm
BPF	Johanson	Pass band: 2400 2500 MHz
Op Amp	Maxim IC	Bias: 3V; GBW: 3 MHz
Controller	TI	Bias: 3V; 10-bit ADC

a free-running VCO was used in this design, coherent demodulation was achieved. The transmit signal and the LO signal used for down-conversion are from the same oscillator. Since the two signals are from the same signal source, their phase noises are closely correlated. The reflected signal is subjected to phase delay, which would be down-converted at mixer to become DC offset that would be canceled by baseband ac-coupling circuitry. The radar sensor baseband circuit is custom-designed with an operational amplifier having a less than 500 KHz cut-off frequency. The added high frequency noises from the environment are uncorrelated, but they have limited impact on radar measured signals because they would be filtered out at radar baseband [17]. The phase noise of the VCO does not affect sensitivity in noncontact vital signs measurement, because of the range correlation effect [16]. Two patch antennas were specifically designed for use in this radar sensor system. The total transmission power was -10 dBm (0.1 mW). In this study, we set the sampling rate of the signal as 100 Hz.

B. Pre-Processing Layer

The preprocessing layer was an RF receiver that received the signal from the sensor layer and down-converted it to baseband I/Q signals. A low-noise amplifier (LNA) was placed at the front end of the preprocessing layer to ensure a favorable noise figure for the receiver chain. The LNA also provided a 19-dB gain to boost the weak signal reflected from the moving target. A ceramic band-pass filter (BPF), as shown in Table I, followed the LNA to block the out-of-band interference. This is critical because an abundance of strong interference is present in the air (e.g., 900-MHz cellular signals and 5.8-GHz WiFi signals). The filtered signal was further boosted by a gain block to reach a sufficient power level for powering the RF port of the demodulator. A quadrature demodulator converted the received signal to baseband I/Q signals, which were amplified by the baseband operational amplifier (Op Amp). The Op Amp was configured with a differential input structure and the baseband gain was determined using the feedback of the amplifier. The Op Amp had a gain bandwidth product of only 3 MHz. Therefore, the Op Amp also served as a low-pass filter that preserved the low-frequency vital signs signals and blocked any interference. The baseband output was digitized using a 10-bit analog-to-digital converter integrated in a microcontroller. After collection using an on-board data acquisition module, the digital baseband I/Q signals were transmitted to a computer for phase demodulation.

C. Modeling Layer

In the $I(t)$ and $Q(t)$ domain, samples of the I/Q signals lie on an ellipse. Therefore, the proposed modeling layer formulates the sampled I/Q signals as an elliptic curve fitting problem and reconstruct radar signal by finding six parameters to represent the ellipse, A, B, C, D, E, G[1]. An ellipse is a special case in conic curves which can be described by (7)

$$F(x, y) = Ax^2 + Bxy + Cy^2 + Dx + Ey + G = 0 \quad (7)$$

with one constraint

$$B^2 - 4AC < 0 \quad (8)$$

where (x, y) are simplified representative coordinates in $I(t)$ and $Q(t)$ space.

To solve the elliptic curve fitting problem from samples of the I/Q signals, we propose ℓ_1 minimization with LMI relaxation. This will be described in the next section. The radar signal parameters (i.e. A_I, A_Q, ϕ_0, DC_I and DC_Q) that describe the transmitted and received signals are derived from the six elliptic parameters. The full derivation from elliptic formulation to radar signal parameters is given in the Appendix. After solving LMI problem and finding six elliptic parameters, the five radar signal parameters (A_I, A_Q, ϕ_0, DC_I and DC_Q) can be calculated using the following equivalences:

$$DC_I = \frac{2CD - BE}{B^2 - 4AC}, \quad (9)$$

[1]For simplicity, we will use $A \sim G$ to represent A, B, C, D, E, G

$$DC_Q = \frac{2AE - BD}{B^2 - 4AC}, \tag{10}$$

$$A_I = \sqrt{\frac{AE^2 + CD^2 + GB^2 - BDE - ACG}{(B^2 - 4AC)\left[\sqrt{(A-C)^2 + B^2} - (A+C)\right]}}, \tag{11}$$

$$A_Q = \sqrt{\frac{AE^2 + CD^2 + GB^2 - BDE - ACG}{(B^2 - 4AC)\left[-\sqrt{(A-C)^2 + B^2} - (A+C)\right]}}, \tag{12}$$

and

$$\phi_0 = \frac{1}{2}\cot^{-1}\left(\frac{A-C}{B}\right). \tag{13}$$

D. Information Layer

The transmitted signal $I(t)$ and received signal $Q(t)$ models were recovered with A_I, A_Q, ϕ_0, DC_I, and DC_Q to increase the accuracy of respiration and heartbeat signal extraction. Chest wall displacement $x(t)$ was identified using the information of gain imbalance (A_I/A_Q) and phase imbalance (ϕ_0) derived from the aforementioned signals. The Gram-Schmit procedure [4] was used to reconstruct $(I(t), Q(t))$ input

$$\begin{bmatrix} I'(t) \\ Q'(t) \end{bmatrix} = \begin{bmatrix} 1 & 0 \\ -\tan\phi_0 & \frac{A_I}{A_Q\cos\phi_0} \end{bmatrix} \begin{bmatrix} I(t) \\ Q(t) \end{bmatrix}. \tag{14}$$

The reconstructed baseband signal is $(I'(t), Q'(t))$

$$I'(t) = A_I\cos\left(\frac{4\pi x(t)}{\lambda}\right) + DC_I, \tag{15}$$

$$Q'(t) = A_I\sin\left(\frac{4\pi x(t)}{\lambda}\right) + \frac{A_I DC_Q}{A_Q\cos\phi_0} - \tan\phi_0 DC_I. \tag{16}$$

Then we can demodulate heart beat and respiration related information, $x(t)$, by the arctangent formula directly

$$x(t) = \arctan\left[\frac{Q'(t) - \frac{A_I DC_Q}{A_Q\cos\phi_0} + \tan\phi_0 DC_I}{I'(t) - DC_I}\right]. \tag{17}$$

Spectral analysis of the demodulated time-variant chest wall movement $x(t)$ was performed to extract two prominent spikes: respiration (low frequency but high amplitude in chest wall movement), and heartbeat (high frequency but low amplitude in chest wall movement). Two band-pass filters with known knowledge of the normal respiration and heartbeat frequency distributions were applied to extract both signals simultaneously (for respiration detection, the BPF was set between 0.05 Hz and 0.5 Hz, and for heartbeat detection, the frequency range was set between 0.5 Hz and 2.5 Hz). Therefore, these BPFs covered ranges of 3–30 respirations per minute (RPM) and 30–150 beats per minute (BPM). The breath and heart rates were determined based on the maximal peak derived from fast Fourier transform by using the Hamming window, and were rounded to the nearest integer to represent the estimated breath and heart rates.

IV. ℓ_1 Minimization With LMI Relaxation to Solve the Elliptic Fitting Problem

A. Preliminary: Model Parameter Identification

There are five unknowns in the radar signal model, (A_I, A_Q, ϕ_0, DC_I and DC_Q). There are two potential methods to identify these unknowns. The first method is based on statistical machine learning [3]. Given a set of labeled inputs, $x(t)$, statistical learning can build up the relationship between unknowns in the model and input signals. When the relationship model is established, it can estimate the values of unknowns with any arbitrary input, $x(t)$. Unfortunately, this method will fail in this application because the Doppler radar signal model is time-varying and non-stationary, which conflicts with the precondition of most of machine learning methods [39]. The second method estimates model parameters based on the signal model (5) and (6) with partial pre-calibration. It is assumed that a prior calibration can be performed on the system such that gain imbalance (the ratio of A_I and A_Q) is 1 and phase imbalance (ϕ_0) is 0. Therefore, the I/Q channel signals will become (18) and (19)

$$I(t) = A_0\cos\left(\frac{4\pi x(t)}{\lambda}\right) + DC_I \tag{18}$$

and

$$Q(t) = A_0\sin\left(\frac{4\pi x(t)}{\lambda}\right) + DC_Q. \tag{19}$$

In this form, there are only three parameters, A_0, DC_I and DC_Q. Note that pairwise samples, $I(n)$ and $Q(n)$, will stay on a circle whose center is (DC_I, DC_Q) and radius is A_0

$$\left(I(t) - DC_I\right)^2 + \left(Q(t) - DC_Q\right)^2 = A_0^2. \tag{20}$$

It is feasible to fit all samples on a circle via least squares optimization [48] and then identify these three unknowns. However, this method is not suitable for automated monitoring applications since it requires calibration of gain/phase imbalance. It is impossible to have a pre-fixed calibration for perfect imbalance compensation in practice.

B. ℓ_2 Minimization Based Fitting

In this work, we attempt to build up the I/Q signal model directly from (5) and (6) and demodulate the phase accurately without precalibration. Given a set of n measurements (I_1, Q_1), (I_2, Q_2), …, (I_n, Q_n), an ellipse can be formed as the following formulation:

$$\begin{aligned} \underset{A\sim G}{\arg\min} \quad & \sum_{i=1}^{n} \|F(I_i, Q_i, A\sim G)\|_2^2 \\ s.t. \quad & B^2 - 4AC < 0 \end{aligned} \tag{21}$$

where the function $F(x, y, A\sim G)$ is defined as the algebraic distance of a point (x, y) to an ellipse parameterized by $A\sim G$.

With the result from (21), we can use (9)–(13) to calculate the five parameters in the signal model from the values of $A\sim G$.

We can see that (21) is in a form of quadratically constrained least squares (min-ℓ_2). In general, it is a NP-hard problem [7] and intractable to obtain the global optimal solution within polynomial time. Fitzgibbon *et al.* [18] transferred the quadratic inequality constraint, $B^2 - 4AC < 0$, into an equality constraint, $4AC - B^2 = 1$, under the assumption that all the points (x, y) are close to an ellipse and all distances $F(x, y)$ are close to zeros

$$\begin{aligned} \arg\min_{A\sim G} \quad & \sum_{i=1}^{n} \|F(I_i, Q_i, A \sim G)\|_2^2 \\ s.t. \quad & 4AC - B^2 = 1. \end{aligned} \tag{22}$$

In this way, the formulation in (22) is well-posed and can be solved by Lagrange regularization and eigenvalue decomposition [18]. There are also some research work under the similar assumption above [25], [41]. However, this method will suffer from the actual scattered data for two reasons. Firstly, when data is noisy and $F(x, y, A \sim G)$ is relatively large, the equality constraint in (22) will not be equivalent to the inequality constraint in (21). Secondly, it is well-known that ℓ_2 minimization based fitting is sensitive to outlier or sparse measurement errors.

According to compressed sensing theory [15] developed in recent years, there are miscellaneous applications indicating that min-ℓ_1 based fitting is more robust to outliers or errors than min-ℓ_2 based fitting [8], [45], [47]. Inspired by this, we consider using min-ℓ_1 for signal model identification as follows:

$$\begin{aligned} \arg\min_{A\sim G} \quad & \sum_{i=1}^{n} \left| x_i^2 A + xyB + y_i^2 C + x_i D + y_i E + G \right| \\ s.t. \quad & B^2 - 4AC < 0 \end{aligned} \tag{23}$$

where (x_i, y_i) denotes the radar measure i. (23) is an ℓ_1 minimization problem with a non-linear constraint and even harder than the quadratically constrained least square problems in (21).

C. Lower-Bound and Linear Matrix Inequality (LMI) Relaxation

In this section, we introduce the method to solve (23) by lower-bound and linear matrix inequality (LMI) relaxation. There are two relaxation steps to solve (23). Firstly, we use the upper bound relaxation to change the objective function. By defining an upper bound distance t_i for each sample (I_i, Q_i), (i.e., $|F(I_i, Q_i, A \sim G)| \le t_i$), we can have the problem with a linear objective function

$$\begin{aligned} \arg\min_{A\sim G, \mathbf{t}} \quad & \sum_{i=1}^{n} t_i \\ s.t. \quad & F(I_i, Q_i, A \sim G) \le t_i \\ & -F(I_i, Q_i, A \sim G) \le t_i \\ & t_i \ge 0, i = 1, \cdots, n \\ & B^2 - 4AC < 0. \end{aligned} \tag{24}$$

By now, the new problem formulation in (24) is still a non-convex problem and unsolvable. Here we apply LMI relaxation by adding a couple of lifting variables and constraints. More specifically, let $v = [1, A, B, C, D, E, G]^T$ be a basis to build a moment matric, M, by $v \times v^T \succeq 0$.

$$\begin{aligned} M &= \begin{bmatrix} 1 & A & B & C & D & E & G \\ A & A^2 & AB & AC & AD & AE & AG \\ B & AB & B^2 & BC & BD & BE & BG \\ C & AC & BC & C^2 & CD & CE & CG \\ D & AD & BD & CD & D^2 & DE & DG \\ E & AE & BE & CE & DE & E^2 & EG \\ G & AG & BG & CG & DG & EG & G^2 \end{bmatrix} \\ &= \begin{bmatrix} 1 & y_1 & y_2 & y_3 & y_4 & y_5 & y_6 \\ y_1 & y_{11} & y_{12} & y_{13} & y_{14} & y_{15} & y_{16} \\ y_2 & y_{12} & y_{22} & y_{23} & y_{24} & y_{25} & y_{26} \\ y_3 & y_{13} & y_{23} & y_{33} & y_{34} & y_{35} & y_{36} \\ y_4 & y_{14} & y_{24} & y_{34} & y_{44} & y_{45} & y_{46} \\ y_5 & y_{15} & y_{25} & y_{35} & y_{45} & y_{55} & y_{56} \\ y_6 & y_{16} & y_{26} & y_{36} & y_{46} & y_{56} & y_{66} \end{bmatrix} \succeq 0 \end{aligned} \tag{25}$$

where

$$\begin{aligned} & y_1 = A,\ y_2 = B,\ y_3 = C,\ y_4 = D,\ y_5 = E, \\ & y_6 = G, \cdots,\ y_{22} = B^2, \cdots,\ y_{13} = AC, \cdots. \end{aligned} \tag{26}$$

Note that a 48×1 unknown, $\mathbf{y}$, and a linear matrix inequality constraint, $M \succeq 0$, are introduced here. As a consequence, we can reformulate (24) as follows:

$$\begin{aligned} \arg\min_{\mathbf{y}, \mathbf{t}} \quad & \sum_{i=1}^{n} t_i \\ s.t. \quad & F(I_i, Q_i, y_1 \sim y_6) \le t_i, \\ & -F(I_i, Q_i, y_1 \sim y_6) \le -t_i, \\ & t_i \ge 0, i = 1, \cdots, n \\ & y_{22} - 4y_{13} < 0 \\ & M \succeq 0. \end{aligned} \tag{27}$$

Note that the moment matrix M is symmetric and positive semidefinite, and the formulation in (27) is convex and can be solved by semi-definite programming [7]. Therefore, we have a feasible solution to identify the signal model with the five unknown parameters.

V. Evaluation

Experimental sets were designed to validate the performance of the system. First, ℓ_1 minimization with LMI relaxation was confirmed to be more robust than ℓ_2 minimization with environmental noise when using simulated data as a test bench. Second, an actuator was employed as a controlled subject for a movement measurement test. Third, a pilot study was conducted on 15 subjects to measure vital signs, including heart and respiratory rates.

A. Empirical Comparison Between ℓ_1 Minimization with LMI Relaxation and ℓ_2 Elliptic Fitting

A simulated data set was developed to quantify the performance of the proposed demodulation method. The data set was

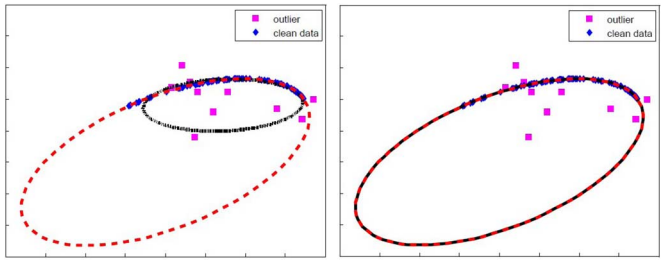

Fig. 5. An example of fitting results on outlier dataset for two algorithms. The outlier percentage is 15% and SNR $= 20$. (a) ℓ_2 based method. (b) ℓ_1 based method.

simulated using known ellipses with noise and outliers. Specifically, the simulated dataset was divided into two classes. One class comprised the simulated data with outliers, and the distance from the outliers to the ellipse ranged up to 50% of the semimajor axis. The other class comprised simulated data with noise, for which the signal-to-noise ratio (SNR) varied from 0.01 to 0.5. In the experiment, the proposed algorithm was applied to perform ellipse fitting on the test bench. The Fitzgibbon ℓ_2 minimization method [18] was used for comparison.

First, the performance of the algorithm when using the outlier data set was evaluated. Fig. 5(a) and (b) show an example of ellipse fitting using the traditional ℓ_2 minimization method and the proposed ℓ_1 minimization method, respectively. The blue dots represent the clean data (zero offset), the red dots represent the outliers, the black curve is the fitting result, and the red dashed curve is the ground truth. Based on this example (15% outliers), the ℓ_1 based algorithm was robust to the red outliers, and the fitted ellipse matched the clean data [Fig. 5(b)]. By contrast, the ℓ_2 based method was affected by the outlier points, and an obvious mismatch existed between the fitted ellipse and the ground truth [Fig. 5(a)].

Both methods with different outlier percentages, ranging from 5% to 40%, were also evaluated. For simplicity, the overlap area between the fitted ellipse and ground-truth ellipse was used to evaluate the matching accuracy [28]. Fig. 7 illustrates two accuracy curves corresponding to these two strategies, and shows that the ℓ_2 based method was sensitive to outliers, whereas the ℓ_1 based method tolerated up to 20% of the outliers.

Second, the performance of the proposed system was tested using a set of data containing Gaussian noise. Fig. 6 illustrates the stability of the ℓ_1 and ℓ_2 algorithms with noise. The SNR ranged from 10 to 100. As the noise levels increased, the deviation from the ground truth for both the algorithms increased (the red ellipse). However, ℓ_1 was still more favorable than ℓ_2 at all SNR levels.

B. Evaluation of the Self-Calibration Function in a Controlled Environment

The performance of the noncontact radar sensing system was tested in this experiment. To evaluate the accuracy of the proposed system, a programmable actuator was used to provide controlled motions. As shown in Fig. 8, a linear actuator (ZABER TNA08A50) and a linear translational stage (ZABER TSB28-1) were placed 1 m from the Doppler radar motion-sensing system. The actuator was programmed to perform a series of standard sinusoidal movements, and the radar system measured and demodulated the actuator motion. To mimic the chest wall movement (by imitating the respiration and heartbeat of humans), an actuator was programmed to perform a simple harmonic back-and-forth motion toward the fixed position radar. The minimal and maximal displacement was set from 0.1 cm to 4 cm, and the movement frequency changed from 0.2 Hz to 2 Hz [21], [38]. The normalized root mean squared (NRMS) error was used to quantify the measurement error.

$$NRMS = \frac{\sum_{i=1}^{n} dist(i)}{n \cdot A} \tag{28}$$

where $dist(i)$ is the distance from the measured point to the sinusoidal curve, and A is the amplitude of movements.

The measured motion was consistent with the presetup harmonic motion of the linear actuator, and the NRMS error was less than 1%. To clearly represent the residual change that occurred when using different magnitudes and frequencies, the results are plotted in Fig. 10. Based on this figure, the average measurement error of the Doppler radar sensing system was less than 3%. This indicates that the measurement error was uncorrelated with movement frequency (in this frequency range) but strongly associated with the movement magnitude. The larger the amplitude of motion, the smaller the measurement error was.

To demonstrate the benefits of self-calibration, the same experiment was conducted in three environments: a lab environment (results presented previously), an outdoor environment, and a corridor on campus. The radar system was initially set up in the lab environment and then moved to the other two locations. These two locations were randomly chosen to demonstrate the portability of a self-calibrating radar. The results in Table II demonstrate the superiority of this proposed modeling layer process. Without enabling self-calibration, when the operating environment changed from the initial location, the NRMS error increased. However, when enabling self-calibration, the NRMS error remained less than 1%. The highest error occurred in the corridor environment because numerous factors cause multipath radar transmission in the long, narrow hallway. Although the proposed methods can be used to calculate radar parameters in real time, manual calibration performed more favorably. According to Table II, manually precalibrating the radar in a lab environment was more effective than using the proposed method. This is because self-calibrated parameters always override a preset default and manual calibration is typically more efficient than fitting-based methods. For the vital signs monitoring application, we are interested in extracting periodic changes from radar signals resulting from relatively slow and periodic respiration and heartbeat events. Therefore, high accuracy chest wall displacement measurement is not required. To measure high accuracy chest wall displacement, manual calibration is still required.

C. Human Vital Signs Measurement with 15 Subjects

Human vital signs derived from radar modulated signals were measured in this experiment. Fifteen subjects were recruited and

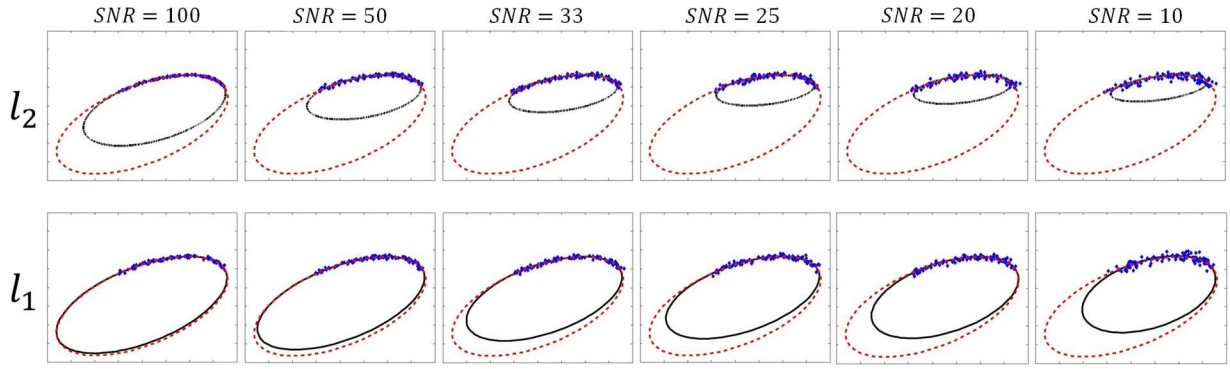

Fig. 6. Fitting results on noisy dataset for two algorithms. SNR ranges from 10 to 100. The first row [from (a) to (f)] is the fitting results of the ℓ_2 based method, and the second row [from (g) to (l)] is the fitting results of the ℓ_1 based method. In each figure, the red dashed curve is the ground truth and the black solid curve is the fitted curve.

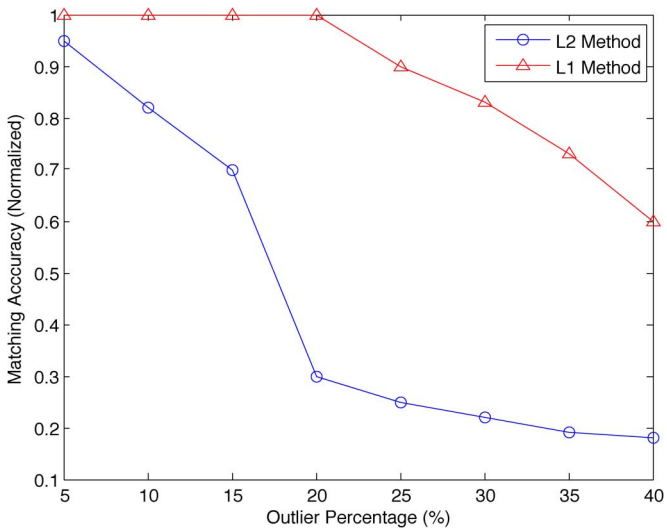

Fig. 7. Two matching accuracy changing curves with different outlier percentages using ℓ_1 based method versus ℓ_2 based method.

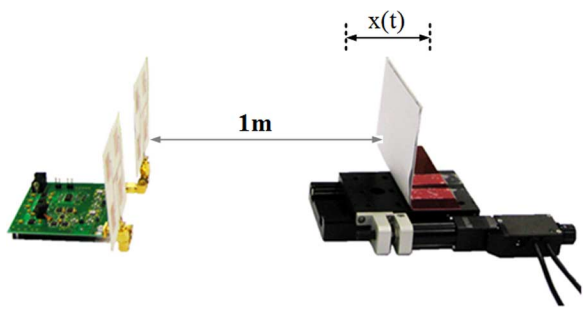

Fig. 8. Experimental setup for measuring the movement of a controlled actuator.

each subject sat in front of the Doppler radar sensor in a lab environment, as shown in Fig. 11. The distance between the subject and the radar sensor varied according to the person. When using the self-calibrating mechanism, tuning the radar for each subject was unnecessary. Each measurement lasted for 120 s, and each subject was tested 3 times. To obtain the breath rate ground truth, a video camera was used to record the chest wall movement (i.e., respiration), and QPS ECG sensor [9] was used to record the waveform of heartbeats. The number of breaths and heartbeats were counted manually within 120 s. Fig. 9 shows the radar measurements and demodulation results for one subject analyzed using the noncontact vital signs measurement system. Both the raw and demodulated data were visualized. A substantial gain imbalance in I/Q signals was observed. Spectral analysis was applied to extract respiration and heartbeat signals. To validate the necessity of the signal-processing method, spectral analysis of the raw radar signal was conducted. In this figure, the Q channel with a phase similar to the demodulated chest wall displacement was chosen. The frequency components of respiration and heartbeat were prominent in the demodulated data spectrum. The demodulated signals were compared with the respiration and heartbeat movements of the subject and were determined to be matched with the ground truth data. The detailed characteristics of the 15 subjects are presented in Table III. Respiration was measured using respiration per minute (RPM), and heartbeat was measured using beat per minute (BPM).

Both respiration and heartbeat signals were extracted and identified using spectral analysis. As shown in Fig. 9, extracting these signals from raw data is difficult. Although respiration can be identified within a range of frequencies (the largest peak in the figure is wider than the other peaks), the heartbeat signal was barely identifiable. In addition, the amplitude of the peak of respiration was much smaller than the spectrum of the demodulated displacement. Voltage rather than centimeters was used to represent the displacement because the radar was not used to measure precise chest wall displacement; instead, the periodic phenomenon of the displacement was identified.

VI. Conclusion and Future Work

In this paper, a noncontact, self-calibrating vital signs measuring system that comprises four layers and is based on Doppler radar was presented. Because this system is self-calibrating, it does not require tuning for each subject. The baseband signals were considered in quadrature and a framework was proposed to automatically analyze $I(t)/Q(t)$ signals, including direct signal modeling, model parameter identification, and demodulation. In this study, signal model identification was formulated into a quadratically constrained ℓ_1 minimization problem and solved using upper-bound and LMI relaxation.

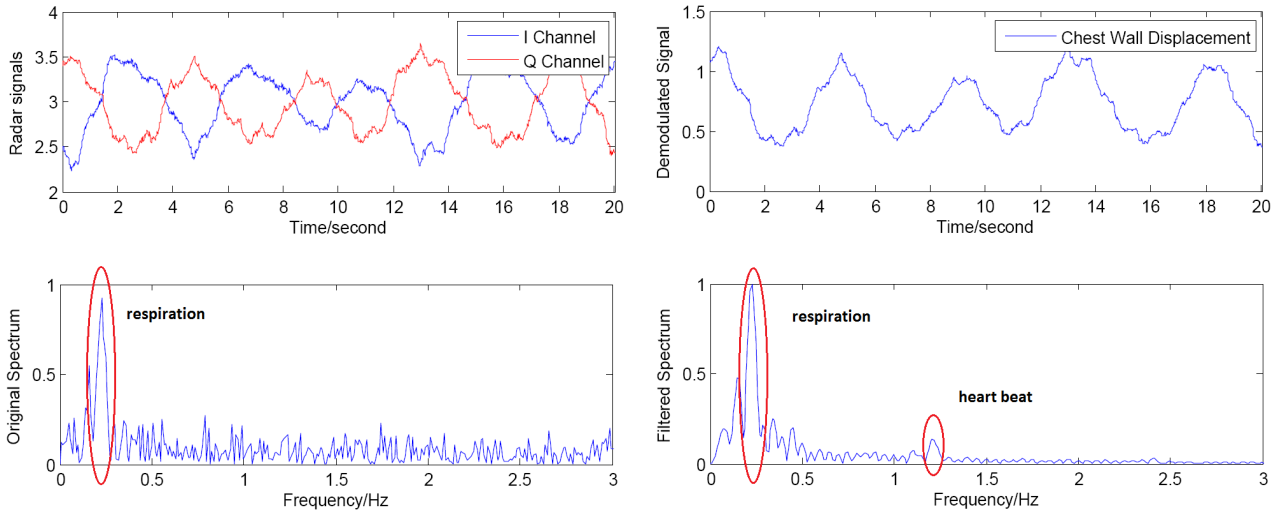

Fig. 9. Comparison of Raw and Demodulated Signals and their respective spectrum analysis for extracting respiration and heartbeat signals.

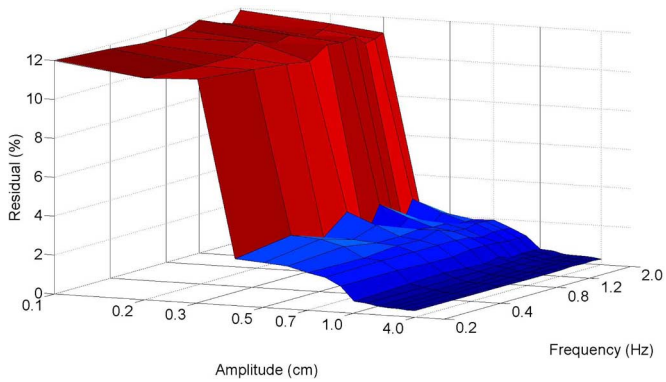

Fig. 10. The residual surface of sinusoidal actuator movement measurement with variations in amplitude and frequency.

TABLE II
ERROR ESTIMATION OF RADAR MEASUREMENT UNDER THREE DIFFERENT ENVIRONMENTS

NRMS(%)	Lab Env	Outdoor	Corridor
with Self-calibration	0.78	0.87	0.92
w/o Self-calibration	0.72	6.21	9.43

Fig. 11. The Doppler radar is measuring vital signs from one subject.

Three sets of experiments were conducted to evaluate the performance of the system. The accuracy and stability of the proposed demodulation framework was demonstrated and the end-to-end performance was examined using real-life scenarios. The results indicated that the system can effectively measure human vital signs without calibrating for each subject.

In the future, the authors will conduct additional comprehensive studies on noninvasive vital signs measurement using larger subject groups. Moreover, the authors will improve the demodulation method for use in more complex application scenarios, such as performing accurate vital signs measurement when subjects are moving quickly.

APPENDIX

In this section, we show that the samples from I/Q channels stay on an ellipse. Given samples $(I(n), Q(n))$

$$I(n) = A_I \cos\left(\frac{4\pi x(n)}{\lambda}\right) + DC_I \tag{29}$$

and

$$Q(n) = A_Q \sin\left(\frac{4\pi x(n)}{\lambda} + \phi_0\right) + DC_Q \tag{30}$$

based on product-to-sum/sum-to-product formulas, we can transform (30) to (32)

$$\frac{I(n) - DC_I}{A_I} = \cos\left(\frac{4\pi x(n)}{\lambda}\right) \tag{31}$$

and

$$\frac{Q(n) - DC_Q}{A_Q} = \sin\left(\frac{4\pi x(n)}{\lambda}\right)\cos(\phi_0) + \cos\left(\frac{4\pi x(n)}{\lambda}\right)\sin(\phi_0). \tag{32}$$

TABLE III
15 SUBJECTS RESPIRATION AND HEARTBEAT EXTRACTION COMPARED WITH GROUND TRUTH (RESP./HEART RATE)

RPM/BPM	Personal Info			Ground Truth			Extracted Data			Error Per Trail		
PID	Sex(M/F)	Height(cm)	Weight(kg)	Trial1	Trial2	Trial3	Trial1	Trial2	Trial3	Trial1	Trial2	Trial3
1	M	170	78	18/72	19/72	18/72	18/72	19/73	18/72	0/0	0/**1**	0/0
2	M	170	71	15/66	15/66	16/65	15/66	15/65	16/65	0/0	0/**1**	0/0
3	M	191	75	17/71	17/72	17/70	17/71	17/72	17/70	0/0	0/0	0/0
4	M	185	83	19/68	19/69	18/67	19/68	20/69	18/67	0/0	**1**/0	0/0
5	M	168	80	14/80	13/82	15/80	14/80	14/81	13/79	0/0	**1/1**	**2/1**
6	F	160	46	20/84	19/84	20/85	20/84	19/84	20/85	0/0	0/0	0/0
7	M	165	73	17/75	17/76	18/76	18/75	17/76	18/76	**1**/0	0/0	0/0
8	F	165	49	15/82	15/82	15/82	15/81	16/82	15/82	0/**1**	**1**/0	0/0
9	M	178	64	12/75	12/75	12/75	12/76	12/75	13/75	0/**1**	0/0	**1**/0
10	M	183	76	18/80	18/79	17/79	18/80	18/79	17/80	0/0	0/0	0/**1**
11	M	175	65	16/63	16/63	17/64	16/63	16/63	17/64	0/0	0/0	0/0
12	M	173	86	19/68	19/69	18/68	17/68	19/69	18/68	**2**/0	0/0	0/0
13	M	173	68	13/74	13/74	13/74	13/74	13/74	12/75	0/0	0/0	**1/1**
14	M	178	81	15/70	15/70	16/71	15/70	15/70	16/71	0/0	0/0	0/0
15	F	165	51	17/82	17/82	17/83	17/82	17/82	18/83	0/0	0/0	**1**/0
Avg(%)	Averaged by number of breath: 17/min and number of heartbeat: 75/min									1.18/0.17	1.18/0.27	1.76/0.27

According to trigonometric identities

$$\sin^2\left(\frac{4\pi x(n)}{\lambda}\right)+\cos^2\left(\frac{4\pi x(n)}{\lambda}\right)=1 \tag{33}$$

we can eliminate $((4\pi x(n))/(\lambda))$ from (31), (32), and (33)

$$\begin{aligned}&\frac{1}{A_I^2}I^2(n)-\frac{2\sin\phi_0}{A_IA_Q}I(n)Q(n)+\frac{1}{A_Q^2}Q^2(n)\\&\quad+f_1(\phi_0,DC_I,DC_Q)I(n)+f_2(\phi_0,DC_I,DC_Q)Q(n)\\&\quad+f_3(\phi_0,DC_I,DC_Q)=0.\end{aligned} \tag{34}$$

Remember that $Ax^2+Bxy+Cy^2+Dx+Ey+G=0$ is a conic curve, and it is an ellipse if and only if $B^2-4AC<0$.

From (34)

$$B^2-4AC=-\frac{4\cos^2(\phi_0)}{A_IA_Q}\le 0. \tag{35}$$

Therefore, we shown that (34) is an ellipse when phase imbalance ϕ_0 is not $(2k+1)\pi/2$. In the case where $\phi_0=(2k+1)\pi/2$, (34) will degenerate into a line.

Furthermore, if the fitted ellipse $F(x,y)=0$ is determined, the parameters in I/Q signal model can be calculated.

$$DC_I=\frac{2CD-BE}{B^2-4AC}, \tag{36}$$

$$DC_Q=\frac{2AE-BD}{B^2-4AC}, \tag{37}$$

$$A_I=\sqrt{\frac{AE^2+CD^2+GB^2-BDE-ACG}{(B^2-4AC)\left[\sqrt{(A-C)^2+B^2}-(A+C)\right]}}, \tag{38}$$

$$A_Q=\sqrt{\frac{AE^2+CD^2+GB^2-BDE-ACG}{(B^2-4AC)\left[-\sqrt{(A-C)^2+B^2}-(A+C)\right]}}, \tag{39}$$

and

$$\phi_0=\frac{1}{2}\cot^{-1}\left(\frac{A-C}{B}\right). \tag{40}$$

REFERENCES

[1] H. Aoki, Y. Takemura, K. Mimura, and M. Nakajima, "Development of non-restrictive ensing system for sleeping person using fibre grating vision sensor.," in *Proc. Int. Symp. Micromechatronics and Human Science*, Nagoya, Japan, Oct. 2001, pp. 155–160.

[2] Beddit [Online]. Available: http://www.beddit.com/

[3] C. Bishop, *Pattern Recognition and Machine Learning*. New York, NY, USA: Springer, 2006.

[4] A. Bjorck, "Solving linear least squares problems by gram-schmidt orthogonalization.," *BIT Numer. Math.*, vol. 7, no. 1, pp. 1–21, Jan. 1967.

[5] A. Blaugrund, "Notes on Doppler-shift lifetime measurements.," *Nucl. Phys.*, vol. 88, no. 3, pp. 501–512, Nov. 1996.

[6] O. Boric-Lukecke, V. Lubecke, B. Park, W. Massagram, and B. Jokanovic, "Heartbeat interval extraction using Doppler radar for health monitoring.," in *Proc. Int. Conf. Telecommunication in Modern Satellite, Cable, Broadcasting Services*, Nis, Berbia, Oct. 2009, pp. 139–142.

[7] S. Boyd and L. Vandenberghe, *Convex Optimization.*. New York, NY, USA: Cambridge Univ. Press, 2004.

[8] E. Candes, J. Romberg, and T. Tao, "Stable signal recovery from incomplete and inaccurate measurements.," *Commun. Pure Applied Math*, vol. 59, no. 4, pp. 1207–1223, Apr. 2006.

[9] Cardiac Direct [Online]. Available: http://www.cardiacdirect.com/

[10] Y. Chekmenev, H. Rara, and A. Farag, "Non-contact, wavelet-based measurement of vital signs using thermal imaging.," in *Proc. ICGST Int. Conf. Graph, Vision and Image Processing*, Cairo, Egypt, Dec. 2005, pp. 25–30.

[11] M. Chen, O. Lubecke, and V. Lubecke, "0.5-um CMOS implementation of analog heart-rate extraction with a robust peak detector.," *IEEE Trans. Instrum. Meas.*, vol. 57, no. 4, pp. 690–698, Apr. 2008.

[12] Y. Chi, P. Ng, E. Kang, J. Kang, J. Fang, and G. Cauwenberghs, "Wireless non-contact cardiac and neural monitoring.," in *Proc. ACM Conf. Wireless Health*, San Diego, CA, USA, Oct. 2010, pp. 15–23.

[13] M. Cretikos, J. Chen, K. Hillman, R. Bellomo, S. Finfer, and A. Flabouris, "The objective medical emergency team activation criteria: A case-control study.," *Resuscitation*, vol. 73, no. 1, pp. 62–72, Jan. 2007.

[14] A. Diaz, M. Bourassa, M. Guertin, and J. Tardif, "Long-term prognostic value of resting heart rate in patients with suspected or proven coronary artery disease.," *Eur. Heart J.*, vol. 26, no. 10, pp. 967–974, Mar. 2005.

[15] D. Donoho, "Compressed sensing.," *IEEE Trans. Inf. Theory*, vol. 52, no. 4, pp. 1289–1306, Apr. 2004.

[16] A. D. Droitcour, O. Boric-Lubecke, V. M. Lubecke, J. Lin, and G. T. A. Kovac, "Range correlation and I/Q performance benefits in single-chip silicon Doppler radars for noncontact cardiopulmonary monitoring," *IEEE Trans. Microw. Theory Tech.*, vol. 52, no. 3, pp. 838–848, Mar. 2004.
[17] A. D. Droitcour, O. Lubecke, V. Lubecke, J. Lin, and G. Kovacs, "Range correlation and I/Q performance benefits in single-chip silicon Doppler radars for noncontact cardiopulmonary monitoring," *IEEE Trans. Microw. Theory Tech.*, vol. 52, no. 3, pp. 557–565, Mar. 2004.
[18] A. Fitzgibbon, M. Pilu, and R. Fisher, "Direct least square fitting of ellipses," *IEEE Trans. Pattern Recog. Mach. Intell.*, vol. 21, no. 5, pp. 476–480, May 1999.
[19] R. Fletcher and J. Han, "Low-cost differential front-end for Doppler radar vital sign monitoring," in *Proc. Int. Microw. Symp. Dig.*, Boston, MA, USA, Jun. 2009, pp. 7–12.
[20] ForaCare [Online]. Available: http://www.foracare.com/
[21] A. Groote, M. Wantier, G. Cheron, M. Estenne, and M. Paiva, "Chest wall motion during tidal breathing," *J. Appl. Phys.*, vol. 83, no. 1, pp. 1531–1537, Jun. 1997.
[22] C. Gu, T. Inoue, and C. Li, "Analysis and experiment on the modulation sensitivity of Doppler radar vibration measurement," *IEEE Microw. Wireless Comp. Lett.*, page in print.
[23] C. Gu, R. Li, R. Fung, C. Torres, S. Jiang, and C. Li, "Accurate respiration measurement using dc-coupled continuous-wave radar sensor for motion-adaptive cancer radiotherapy," *IEEE Trans. Biomed. Eng.*, vol. 59, no. 11, pp. 3117–3123, Nov. 2012.
[24] C. Gu, W. Xu, G. Wang, J. A. Rice, L. Ran, and C. Li, "Noncontact large-scale displacement tracking: Doppler radar for water level gauging," *IEEE Microw. Wireless Comp. Lett.*, vol. 24, no. 12, pp. 899–901, Dec. 2014.
[25] R. Halir and J. Flusser, Numerically Stable Direct Least Squares Fitting of Ellipses, 1998.
[26] D. Heise and M. Skubic, "Monitoring pulse and respiration with a non-invasive hydraulic bed sensor," in *Proc. Conf. IEEE Eng. Med. Biol. Soc.*, pp. 2119–2123, 20010.
[27] A. Huang, W. Xu, Z. Li, L. Xie, M. Sarrafzadeh, X. Li, and J. Cong, "System light-loading technology for mhealth: Manifold-learning based medical data cleansing and clinical trials in we-care project," *IEEE J. Biomed. Health Informat.*, vol. 18, no. 5, pp. 1581–1589, Sep. 2014.
[28] G. Hughes and M. Chraibi, Calculating Ellipse Overlap Areas, ArXiv eprints 1106.37.87, pp. 1–49, 2011.
[29] C. Lee, C. Yoon, H. Kong, H. C. Kim, and Y. Kim, "Heart rate tracking using a Doppler radar with the reassigned joint time-frequency transform," *IEEE Antennas Wireless Propag. Lett.*, vol. 10, no. 5, pp. 1096–1099, May 2011.
[30] C. Li and J. Lin, "Random body movement cancellation in Doppler radar vital sign detection," *IEEE Trans. Microw. Theory Tech.*, vol. 56, no. 12, pp. 3143–3152, Dec. 2008.
[31] C. Li, Y. Xiao, and J. Lin, "Experiment and spectral analysis of a low-power ka-band heartbeat detector measuring from four sides of a human body," *IEEE Trans. Microw. Theory Tech.*, vol. 54, no. 12, pp. 4464–4471, Dec. 2006.
[32] J. Lin, "Microwave sensing of physiological movement and volume changes: A review," *Bioelectromagnetics*, vol. 13, no. 3, pp. 557–565, Nov. 1992.
[33] J. J. Liu, W. Xu, M.-C. Huang, N. Alshurafa, M. Sarrafzadeh, N. Raut, and B. Yadegar, "A dense pressure sensitive bedsheet design for unobtrusive sleep posture monitoring," in *Proc. IEEE Int. Conf. Pervasive Computing and Communications*, San Diego, CA, USA, Mar. 2013, pp. 207–215.
[34] W. Massagram, V. Lubecke, A. Madsen, and O. Boric-Lubecke, "Assessment of heart rate variability and respiratory sinus arrhythmia via Doppler radar," *IEEE Trans. Microw. Theory Tech.*, vol. 57, no. 10, pp. 2542–2549, Oct. 2009.
[35] Omron Inc. [Online]. Available: http://www.omronhealthcare.com/
[36] B. Park, O. Lubecke, and V. Lubecke, "Arctangent demodulation with dc offset compensation in quadrature Doppler radar receiver systems," *IEEE Trans. Microw. Theory Tech.*, vol. 55, no. 5, pp. 1073–1079, May 2007.
[37] B. Park, S. Yamada, and V. Lubecke, "Measurement method for imbalance factors in direct-conversion quadrature radar systems," *IEEE Microw. Wireless Compon. Lett.*, vol. 17, no. 5, pp. 403–405, May 2007.
[38] G. Ramachandran and M. Singh, "Three-dimensional reconstruction of cardiac displacement patterns on the chest wall during the P, QRS, T-segments of the ECG by laser speckle interferometry," *Med. Bioeng. Comput.*, vol. 27, no. 1, pp. 525–530, Jun. 1989.
[39] C. Rasmussen and K. Williams, *Gaussian Processes for Machine Learning*. Cambridge, MA, USA: MIT Press, 2006.
[40] M. Steffen, A. Aleksandrowicz, and S. Leonhardt, "Mobile noncontact monitoring of heart and lung activity," *IEEE Trans. Biomed. Circuits Syst.*, vol. 1, no. 4, pp. 250–257, Dec. 2007.
[41] Z. Szpak, W. Chojnachi, and A. Hegel, "Guaranteed ellipse fitting with the Sampson distance," in *Proc. 12th Eur. Conf. Computer Vision*, Firenze, Italy, Oct. 2012, pp. 18–23.
[42] Y. Tao, J. Long, J. Wang, W. Cui, W. Ma, J. Huangfu, and L. Ran, "A novel non-contact vital sign detection system based on phase-coded pulse radar," in *Proc. IET Conf. Wireless Mobile and Computing*, Hangzhou, China, Dec. 2009, pp. 421–424.
[43] E. Valchinov and N. Pallikarakis, "An active electrode for biopotential recording from small localized bio-sources," *BioMed. Eng. OnLine*, vol. 3, no. 1, p. 25, 2004.
[44] K. Watanabe, T. Watanabe, H. Tatanabe, H. Ando, and T. Ishikawa, "Noninvasive measurement of heartbeat, respiration, snoring and body movements of a subject in bed via a pneumatic method," *IEEE Trans. Biomed. Eng.*, vol. 52, no. 12, pp. 2100–2107, Dec. 2005.
[45] W. Xu, C. Gu, C. Li, and M. Sarrafzadeh, "Robust Doppler radar demodulation via compressed sensing," *IET Electron. Lett.*, vol. 48, no. 22, pp. 1428–1430, Oct. 2012.
[46] W. Xu, Z. Li, M.-C. Huang, N. Amini, and M. Sarrafzadeh, "ecushion: An etextile device for sitting posture analysis," in *Proc. IEEE Conf. Implantable and Wearable Body Sensor Networks*, Dallas, TX , USA, May 2011, pp. 194–199.
[47] W. Xu, M. Zhang, A. Sawchuk, and M. Sarrafzadeh, "Robust human activity and sensor location co-recognition via sparse signal representation," *IEEE Trans. Biomed. Eng.*, vol. 58, no. 11, pp. 1–10, Nov. 2012.
[48] M. Zakrzewski, H. Raittinen, and J. Vanhala, "Comparison of center estimation algorithms for heart and respiration monitoring with microwave Doppler radar," *IEEE Sensors J.*, vol. 12, no. 3, pp. 627–634, Mar. 2012.
[49] Z. Zhu, J. Fei, and I. Pavlidis, "Tracking humane breath in infrared imaging," in *Proc. IEEE Symp. Bioinformatics and Bioengineering*, Washington, DC, Jul. 2005, pp. 227–231.
[50] Z. Zhu and X. Huang, "Bias analysis of a gain/phase/dc-offset estimation technique for direct frequency conversion modulators," in *Proc. IEEE Int. Conf. Acoustics, Speech, Signal Processing*, Ottawa, ON, Canada, Mar. 2005, pp. 18–23.
[51] D. Zito, D. Pepe, M. Mincica, F. Zito, A. Tognetti, A. Lanata, and D. De Rossi, "SoC CMOS UWB pulse radar sensor for contactless respiratory rate monitoring," *IEEE Trans. Biomed. Circuits Syst.*, vol. 5, no. 6, pp. 503–510, Dec. 2011.

Ming-Chun Huang (M'14) received the Ph.D. degree in computer science from the University of California, Los Angeles, Los Angeles, CA, USA.

Currently, he is an Assistant Professor in the Electrical Engineering and Computer Science Department, Case Western Reserve University, Cleveland, OH, USA. He has multiple years experience in pressure sensitive medical devices development, pressure map analysis, and physiological signal extraction research. He is an expert in mHealth, telemedicine, and noninvasive sensing system design. His board research interests include the area of wearable computing, health informatics, big data analysis, human computer interaction, sensor, network, augmented reality, and applications of Internet of Things.

Dr. Huang received the Best Medical and Performance Application Paper Award from the IEEE Conference on Implantable and Wearable Body Sensor Networks in 2013 and the Best Demonstration Award in ACM Wireless Health Conference in 2011.

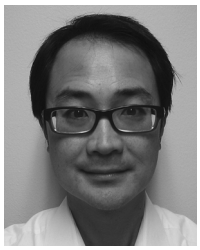

Jason J. Liu (M'14) received the B.Sc. degree in computer science and the B.E. degree in electrical engineering (first class honors) from the University of Sydney, Sydney, Australia, the M.S.E. degree in robotics from the University of Pennsylvania, Philadelphia, PA, USA, and the Ph.D. degree in computer science from the University of California, Los Angeles, Los Angeles, CA, USA.

His research interests include computer vision, machine learning, medical informatics, wireless health, and human-computer interaction. Currently, he is a Research Scientist at Northrop Grumman, Redondo Beach, CA.

Dr. Liu received the Best Paper Award at the IEEE Conference on Implantable and Wearable Body Sensor Networks in 2013.

Wenyao Xu (M'13) received the Ph.D. degree from the Department of Electrical Engineering, University of California, Los Angeles, Los Angeles, CA, USA, in 2013.

Currently, he is an Assistant Professor in the Computer Science and Engineering Department, State University of New York at Buffalo, Buffalo, NY, USA. His current research interests include embedded system design, computational modeling, algorithm design, human computer interaction, integrated circuit design technologies, and their applications in medical and health applications.

Dr. Xu received the Best Medical and Performance Application Paper Award from the IEEE Conference on Implantable and Wearable Body Sensor Networks in 2013 and the Best Demonstration Award from the ACM Wireless Health Conference in 2011.

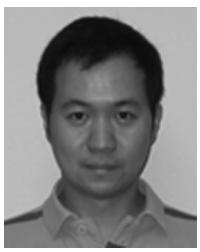

Changzhan Gu (M'13) received the B.S. and M.S. degrees in information and electronic engineering from Zhejiang University, Hangzhou, China, in 2006 and 2008, respectively, the M.S. degree in electrical engineering from the University of Florida, Gainesville, FL, USA, in 2010, and the Ph.D. degree in electrical engineering from Texas Tech University, Lubbock, TX, USA, in 2013.

From June 2013 to January 2014, he was a Senior RF Systems Engineer with MaxLinear Inc., Irvine, CA, USA, where he was involved with satellite TV tuner system-on-chip (SoC). Since January 2014, he has been a Senior Engineer with Marvell Technology Group Ltd., Santa Clara, CA, USA, where he is involved with the reference design for wireless connectivity SoC including both standalone and combo WiFi/Bluetooth/NFC silicon solutions. His research interests include RF and microwave circuits/systems, RF SoC, wireless sensing technologies, and the biomedical applications of RF/microwave.

Dr. Gu was the recipient of seven IEEE conference Best Paper Awards as an author/coauthor. As lead author, he was the recipient of Best Paper Awards of IEEE RWW in 2011 to 2013. He was also the recipient of the IEEE Microwave Theory and Techniques Society (MTT-S) 2013 Graduate Fellowship for Medical Applications, the 2013 Texas Tech Horn Professors Graduate Achievement Award, and the 2012 Chinese Government Award for Outstanding Self-Financed Students Abroad.

Changzhi Li (M'09–SM'14) received the B.S. degree in electrical engineering from Zhejiang University, Zhejiang, China,, and the Ph.D. degree in electrical engineering from the University of Florida, Gainesville, FL, USA, in 2004 and 2009, respectively.

In the summers of 2007 and 2009, he was with Alereon Inc. and Coherent Logix Inc., both in Austin, TX, USA, where he was involved with ultrawideband (UWB) transceivers and software-defined radio. In 2009, he joined Texas Tech University, Lubbock, TX, USA, as an Assistant Professor and became an Associate Professor in 2014. His research interests include biomedical applications of microwave/RF, wireless sensor, and RF/analog circuits.

Dr. Li is an Associate Editor for the IEEE TRANSACTIONS ON CIRCUITS AND SYSTEMS—II: EXPRESS BRIEFS. He served as the TPC Cochair for the IEEE Wireless and Microwave Technology Conference (WAMICON) in 2012 and 2013. He received the ASEE Frederick Emmons Terman Award in 2014, the IEEE-HKN Outstanding Young Professional Award in 2014, the NSF Faculty Early CAREER Award in 2013, and the IEEE MTT-S Graduate Fellowship Award in 2008. He received nine best conference/student paper awards as author/advisor in the IEEE Radio and Wireless Week (RWW) and the IEEE WAMICON.

Majid Sarrafzadeh (F'96) received the Ph.D. degree in electrical and computer engineering from the University of Illinois at Urbana-Champaign, Champaign. IL, USA, in 1987.

He joined Northwestern University, Evanston, IL, USA, as an Assistant Professor in 1987. In 2000, he joined the Computer Science Department, University of California, Los Angeles (UCLA), Los Angeles, CA, USA. He is a cofounder and codirector of the UCLA Wireless Health Institute (WHI). His recent research interests lie in the area of embedded computing with emphasis on healthcare. He has authored approximately 400 papers, coauthored five books, and is a named inventor on many U.S. patents. He has collaborated with many industries for the past 25 years. He cofounded two companies circa 2000 and both were acquired circa 2004. He recently cofounded MediSens and Bruin Biometrics, both concentrate in the area of technology in healthcare.